# Polarimetry in turbid, birefringent, optically active media: A Monte Carlo study of Mueller matrix decomposition in the backscattering geometry

Nirmalya Ghosh,[1] Michael F. G. Wood,[1] and I. Alex Vitkin[2,a)]
[1]*Division of Biophysics and Bioimaging, Ontario Cancer Institute, University Health Network, 610 University Avenue, Toronto, Ontario M5G 2M9, Canada and Department of Medical Biophysics, University of Toronto, 610 University Avenue, Toronto, Ontario M5G 2M9, Canada*
[2]*Division of Biophysics and Bioimaging, Ontario Cancer Institute, University Health Network, 610 University Avenue, Toronto, Ontario M5G 2M9, Canada and Department of Medical Biophysics and Radiation Oncology, University of Toronto, 610 University Avenue, Toronto, Ontario M5G 2M9, Canada*

(Received 12 March 2008; accepted 19 August 2008; published online 19 May 2009)

Determination of the intrinsic polarization properties of a complex turbid medium such as biological tissue in the backscattering geometry (a geometry that is convenient for *in situ* applications) is complicated due to the confounding influence of scattering, and due to simultaneous occurrence of several polarization effects. We have investigated the polar decomposition approach of Mueller matrices to delineate individual intrinsic polarization parameters (specifically linear retardance $\delta$ and optical rotation $\psi$) of a birefringent, chiral, turbid medium in the backscattering geometry, using Mueller matrices generated with polarization-sensitive Monte Carlo simulations. The results show that near the exact backscattering direction, the interplay of the scattering-induced linear retardance and diattenuation on the intrinsic values for $\delta$ and $\psi$ is coupled in a complex interrelated way, due to contribution of the backscattered photons. In contrast, these effects were significantly reduced for detection positions at distances larger than a transport length away from the point of illumination. Simultaneous determination of the intrinsic values for $\delta$ and $\psi$ of a birefringent, chiral, turbid medium in the backward detection geometry can thus be accomplished by decomposing the Mueller matrices recorded at distances larger than a transport length away from the point of illumination. Determination of the intrinsic values for these polarization parameters in backscattering geometry could be significant in, for example, for quantification of tissue structural anisotropy and for noninvasive blood glucose measurements of diabetic patients. © *2009 American Institute of Physics*. [DOI: 10.1063/1.3116129]

## I. INTRODUCTION

Studies of polarization properties of scattered light from turbid media such as biological tissues have received considerable attention because of their potential applications in diagnostic photomedicine.[1] Polarization properties of scattered light from tissue contain rich morphological and functional information on tissue and its underlying structure. For example, the anisotropic organized nature of many tissues stemming from their fibrous structure leads to linear birefringence (or linear retardance), manifest as anisotropic refractive indices parallel and perpendicular to the fibers. Muscle fibers and extracellular matrix proteins (such as collagen and elastin) possess this fibrous structure and accordingly exhibit linear birefringence. Changes in this anisotropy resulting from disease progression or treatment response alter the optical birefringence properties, making this a potentially sensitive probe of tissue status.[2–4] Glucose, another important tissue constituent, exhibits circular birefringence due to its asymmetric chiral structure. Its presence in tissue leads to rotation of the plane of linearly polarized light about the axis of propagation (known as optical rotation or optical activity).[5–10] Although a wealth of interesting tissue properties can potentially be probed with polarized light, the complex light-tissue interactions (particularly the strong multiple scattering effects) present formidable challenges, both in terms of accurate measurement and in terms of data analysis/interpretation.

The Mueller matrix represents the transfer function of an optical system in its interactions with polarized light, the elements reflecting various sample properties of potential interest.[11,12] However, in complex turbid media such as tissues, many optical polarization effects occur simultaneously (such as depolarization, linear birefringence, and optical activity) and contribute in a complex interrelated way to the Mueller matrix elements. Hence, these represent several "lumped" effects, masking potentially interesting ones and hindering unique data interpretation. The challenges are thus to minimize or compensate for multiple scattering, and to decouple the individual contributions of simultaneously occurring polarization effects. Each of the individual processes, if separately extracted from the lumped system Mueller matrix, can potentially be used as a useful biological metric.

We have recently investigated the use of an expanded Mueller matrix decomposition method to tackle this prob-

a)Author to whom correspondence should be addressed. Electronic mail: vitkin@uhnres.utoronto.ca. Tel.: +1-416-946-2990. FAX: +1-416-946-6529.

 © 2009 American Institute of Physics

Downloaded 08 Oct 2009 to 146.139.50.17. Redistribution subject to AIP license or copyright; see http://jap.aip.org/jap/copyright.jsp

lem. Preliminary studies demonstrated that the decomposition approach can successfully delineate individual intrinsic polarization parameters of a complex turbid medium in the forward detection geometry.[13] Yet the backward detection geometry is more convenient than the forward detection geometry for many practical applications (particularly for *in situ* measurements). However, the influence of the scattering-induced effects on the intrinsic polarization parameters of a medium is more pronounced in this geometry due to the contribution of the backscattered (singly or weakly scattered) photons.[14,15] This Mueller matrix decomposition method has previously been explored for the determination of optical rotation from chiral turbid medium in the backscattering geometry.[16] However, in order to realize the potential of the Mueller matrix decomposition approach for quantification and interpretation of all the intrinsic polarization parameters (specifically linear retardance $\delta$ and optical rotation $\psi$) in the backscattering geometry from a complex turbid medium such as tissue, it is necessary to have quantitative understanding of the confounding effects of scattering, the propagation path of multiply scattered photons and detection position on the Mueller matrix-derived polarization parameters. This has not been previously investigated. We are therefore investigating the Mueller matrix decomposition method to tease out individual intrinsic polarization parameters of a birefringent, chiral, turbid medium in the backward detection geometry, using Mueller matrices generated with a polarization-sensitive Monte Carlo simulation model. The results of these theoretical investigations are reported in this paper.

The organization of this paper is as follows. The forward polarization-sensitive Monte Carlo model and the inverse process for polar decomposition of the resulting Mueller matrices are described in Sec. II. The decomposition results in the backward detection geometry from turbid media having varying optical properties are presented in Sec. III. By radially offsetting the detection point, a possible strategy for simultaneous determination of the intrinsic values for linear retardance ($\delta$) and optical rotation ($\psi$) is also discussed. The paper concludes with a discussion on the implications of these results in diagnostic photomedicine.

## II. THEORY

### A. Forward modeling: Polarization-sensitive Monte Carlo simulations

A polarization-sensitive Monte Carlo simulation model, developed in our group,[17] was used to generate the Mueller matrices of scattered light exiting the medium in the backscattering direction. The model's testing and experimental validation have previously been reported.[15,18] In the simulations, the photons are propagated between scattering events, as determined by pseudorandom sampling of scattering mean free path, similar to conventional Monte Carlo model for light propagation in a multiply scattering medium.[19] The phase function, calculated from Mie theory,[20] is used for sampling the scattering angles and computing the polarization changes in photons after successive scattering events. The polarization information (in the form of Stokes vectors) is tracked for each photon packet. The scattering histories of a large number of such packets are tracked as they propagate through the medium and are summed to yield the macroscopic polarization parameters of interest (Stokes vectors, Mueller matrices, and pathlength distributions). Our polarization-sensitive Monte Carlo model[17] has been extended to simulate the simultaneous effects of linear birefringence and optical activity in the presence of turbidity employing the Jones $N$-matrix formalism.[21,22] Here, the matrix of the sample is represented as an exponential sum of differential matrices, known as $N$-matrices. Each matrix in this sum corresponds to a single optical property (e.g., linear birefringence or optical activity). These $N$-matrices are then used to express the matrix for the combined effect. The resulting matrix is applied to the photon between scattering events to model the simultaneous occurrence of linear birefringence and optical activity in a scattering medium. This formalism overcomes the issue of noncommutative Mueller matrices ($\mathbf{M_A M_B} \neq \mathbf{M_B M_A}$) for the individual polarization effects and can accurately model the simultaneous occurrence of many polarization effects in a turbid medium. The details of this formalism have been published.[18]

Simulations were run for a set of input optical parameters of the scattering medium. Mie theory was used to compute the scattering phase function for known diameter ($D$) and refractive index of scatterer ($n_s$) and refractive index of the surrounding medium ($n_m$). The wavelength of light ($\lambda$) was chosen to be $\lambda = 632.8$ nm. The computed phase function, the scattering coefficient ($\mu_s$), and absorption coefficient ($\mu_a$) of the medium were then used in the simulations. The absorption was selected to be small ($\mu_a = 0.0001\ \text{mm}^{-1}$) for all simulations. Circular and linear birefringences were modeled through the optical activity $\chi$ in deg/cm, and through the anisotropy in refractive indices ($\Delta n$). Here, $\Delta n (= n_e - n_o)$ is the difference in refractive index along the extraordinary axis ($n_e$) and the ordinary axis ($n_o$). In this formalism, it is assumed that the medium is uniaxial and that the direction of the extraordinary axis and the value for $\Delta n$ is constant throughout the scattering medium. In each simulation, $n_e$ and $n_o$ were taken as input parameters, and a specific direction of the extraordinary axis was chosen. As each photon propagates between scattering events, the difference in refractive indices seen by the photon depends on the propagation direction with respect to the extraordinary axis. The effect was modeled using standard formulas describing the angular variation of refractive index in uniaxial medium.[18] The state of polarization of incident light was changed sequentially to horizontal (Stokes vector $[1\ 1\ 0\ 0]^T$), vertical ($[1\ -1\ 0\ 0]^T$), $+45^\circ$ ($[1\ 0\ 1\ 0]^T$) linear polarization, and circular polarization ($[1\ 0\ 0\ 1]^T$), and the Stokes vectors *[I Q U V]* of light exiting the sample were recorded for each given incident polarization state. The Mueller matrix was generated by performing simple algebraic manipulations using the recorded output Stokes parameters for each respective input state.[11,13]

The Mueller matrices were generated for a 1-cm-thick slab of scattering medium having varying optical properties ($\mu_s$, $\Delta n$, and $\chi$), for light exiting the medium through the backward direction. The photon collection geometry was

Downloaded 08 Oct 2009 to 146.139.50.17. Redistribution subject to AIP license or copyright; see http://jap.aip.org/jap/copyright.jsp

chosen to have a detection area of 1 $mm^2$ and an acceptance angle of 20°. These selected parameters mimic our experimental polarimetry platform.[13,14,18]

### B. Inverse problem: Polar decomposition of the Mueller matrix

Polar decomposition method consists of decomposing a given Mueller matrix **M** into the product of three "basis" matrices,[23]

$$\mathbf{M} = \mathbf{M_\Delta} \cdot \mathbf{M_R} \cdot \mathbf{M_D}, \tag{1}$$

representing a depolarizer matrix $\mathbf{M_\Delta}$ to account for the depolarizing effects of the medium, a retarder matrix $\mathbf{M_R}$ to describe the effects of linear birefringence and optical activity, and a diattenuator matrix $\mathbf{M_D}$ to include the effects of linear and circular diattenuations.

The three basis Mueller matrices thus determined can then be further analyzed to yield a wealth of independent constituent polarization parameters.[13,16] Specifically, diattenuation ($d$, differential attenuation of orthogonal polarizations for both linear and circular polarization states), depolarization coefficient ($\Delta$, linear and circular), linear retardance ($\delta$, difference in phase between two orthogonal linear polarization, and its orientation angle with respect to the horizontal axis$=\theta$), and circular retardance or optical rotation ($\psi$, difference in phase between right and left circularly polarized light) can be determined from the decomposed basis matrices.

Proceeding as outlined above, the magnitude of diattenuation ($d$) can be determined as[23]

$$d = \{1/\mathbf{M_D}(1,1)\} \times [\{\mathbf{M_D}(1,2)\}^2 + \{\mathbf{M_D}(1,3)\}^2 + \{\mathbf{M_D}(1,4)\}^2]^{1/2}, \tag{2}$$

Here where $\mathbf{M}$ $(i,j)$ are the elements of the $4\times4$ Mueller matrix. The coefficients $\mathbf{M_D}$ (1,2) and $\mathbf{M_D}$ (1,3) represent linear diattenuation for horizontal (vertical) and +45° (−45°) linear polarization, respectively, and the coefficient $\mathbf{M_D}$ (1,4) represents circular diattenuation.

Turning to depolarization, the diagonal elements of the decomposed matrix $\mathbf{M_\Delta}$ can be used to calculate the depolarization coefficients [$\mathbf{M_\Delta}$ (2,2) and $\mathbf{M_\Delta}$ (3,3) are depolarization coefficients for incident horizontal (or vertical) and 45° (or −45°) linearly polarized light, and $\mathbf{M_\Delta}$ (4,4) is the depolarization coefficient for incident circularly polarized light]. The net depolarization coefficient $\Delta$ is defined as[23]

$$\Delta = 1 - \{|\mathrm{tr}(\mathbf{M_\Delta}) - 1|/3\}. \tag{3}$$

Finally, the following analysis can be performed on the retardance matrix $\mathbf{M_R}$. $\mathbf{M_R}$ can be further expressed as a combination of a matrix for a linear retarder (having a magnitude of linear retardance $\delta$, its retardance axis at angle $\theta$ with respect to the horizontal) and a circular retarder (optical rotation with magnitude of $\psi$).[16] Using the known functional form of the linear retardance and optical rotation matrices, the values for optical rotation ($\psi$) and linear retardance ($\delta$) can be determined from the elements of the matrix $\mathbf{M_R}$ as[13,16]

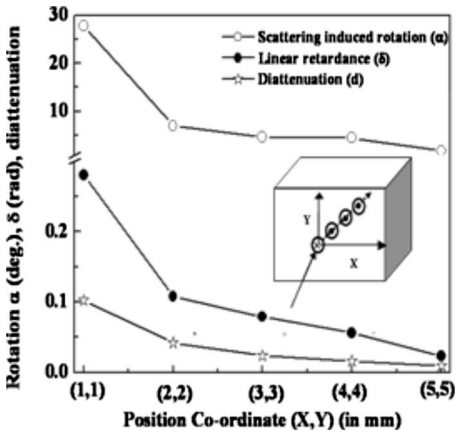


FIG. 1. The Monte Carlo-generated variation of scattering induced rotation $\alpha$ as a function of distance from the point of illumination of a nonbirefringent ($\Delta n=0$), achiral ($\chi=0°\ cm^{-1}$), turbid medium ($\mu_s=6\ mm^{-1}$, $g=0.935$, and thickness $t=10$ mm) comprised of monodispersed spherical scatterers ($D=1.40\ \mu$m, $n_s=1.59$, and $n_m=1.34$). The incident light was horizontally polarized (Stokes vector $[1\ 1\ 0\ 0]^T$) and the rotation values $\alpha$ were calculated using Eq. (6) on the recorded Stokes parameters *[I Q U V]* of light exiting the sample through the backscattering plane. The variation of the decomposition-derived diattenuation $d$ (which is the origin of the scattering induced rotation) is also shown, as is the variation of the scattering induced linear retardance $\delta$. The inset displays the detection positions in the backscattering plane ($X$-$Y$ plane, $Z=0$).

$$\psi = \tan^{-1}[\{\mathbf{M_R}(3,2) - \mathbf{M_R}(2,3)\}/\{\mathbf{M_R}(2,2) + \mathbf{M_R}(3,3)\}], \tag{4}$$

$$\delta = \cos^{-1}\{[(\mathbf{M_R}(2,2) + \mathbf{M_R}(3,3))^2 + (\mathbf{M_R}(3,2) - \mathbf{M_R}(2,3))^2]^{1/2} - 1\}. \tag{5}$$

Note that the multiplication order in Eq. (1) is ambiguous (due to the noncommuting nature of matrix multiplication, as per the $N$-matrix forward modeling discussion), so that six different decompositions are possible. It has been shown that the matrix product in Eq. (1) or its reverse order ($\mathbf{M} = \mathbf{M_D}\mathbf{M_R}\mathbf{M_\Delta}$) always leads to a physically realizable Mueller matrix.[24,25] The Monte Carlo-generated Mueller matrices were therefore decomposed following either the order of Eq. (1) or its reverse. Importantly, the three useful polarization parameters [$\Delta$, $\psi$, and $\delta$, derived through Eqs. (3)–(5)] of the turbid media were found to be independent of the order and were similar for decomposition using either Eq. (1) or the reverse order (difference in the values for the polarization parameters obtained through either the forward or the reverse order decomposition were in the range 1%–5%).

## III. RESULTS AND DISCUSSION

The determination of the intrinsic values for linear retardance ($\delta$) and optical rotation ($\psi$) of a birefringent, chiral, turbid medium in the backward detection geometry is complex due to the confounding influence of the scattering-induced effects.[14,15] Significant contribution of large angle scattered (backscattered) photons in this geometry leads to apparently large magnitude of rotation of linear polarization vector even in the absence of chirality.[15] This is illustrated in Fig. 1, where the Monte Carlo-generated variation of scattering induced rotation $\alpha$ is displayed as a function of distance

Downloaded 08 Oct 2009 to 146.139.50.17. Redistribution subject to AIP license or copyright; see http://jap.aip.org/jap/copyright.jsp

TABLE I. Top: The Monte Carlo simulation generated Mueller matrix [matrix 2 of Eq. (8), corresponding to detection point (2) with position coordinate (2, 0), $Z=0$] and the decomposed basis matrices for a nonbirefringent ($\Delta n=0$), achiral ($\chi=0^\circ$ cm$^{-1}$), turbid medium ($\mu_s=6$ mm$^{-1}$ and $g=0.935$). Bottom: The values for the different polarization parameters extracted from the decomposed matrices via Eqs. (2)–(5).

$$\mathbf{M}=\begin{pmatrix} 1.0 & -0.0690 & 0.002 & -0.0034 \\ -0.0666 & 0.2192 & 0.0012 & -0.0035 \\ -0.0004 & 0.0018 & 0.1407 & -0.0535 \\ 0.0012 & -0.0012 & 0.0568 & 0.4674 \end{pmatrix}$$

$$\mathbf{M}_\Delta=\begin{pmatrix} 1.0 & 0 & 0 & 0 \\ -0.0517 & 0.2156 & 0 & 0 \\ -0.0005 & 0 & 0.1460 & 0 \\ 0.0027 & 0 & 0 & 0.4735 \end{pmatrix}$$

$$\mathbf{M}_\mathbf{R}=\begin{pmatrix} 1.0 & 0 & 0 & 0 \\ 0 & 1.0 & -0.0006 & -0.0034 \\ 0 & 0 & 0.9839 & -0.1785 \\ 0 & 0.0034 & 0.1785 & 0.9839 \end{pmatrix}$$

$$\mathbf{M}_\mathbf{D}=\begin{pmatrix} 1.0 & -0.0690 & 0.0002 & -0.0034 \\ -0.0690 & 1.0 & -0 & 0.0001 \\ 0.0002 & -0 & 0.9976 & -0 \\ 0.0034 & 0.0001 & -0 & 0.9976 \end{pmatrix}$$

| Parameters | Estimated values |
|---|---|
| $d$ | 0.069 |
| $\Delta$ | 0.722 |
| $\psi$ | 0.009° |
| $\delta$ | 0.179 rad |

from the point of illumination of a nonbirefringent (anisotropy in refractive index $\Delta n=0$), achiral (optical activity $\chi=0^\circ$ cm$^{-1}$), turbid medium ($\mu_s=6$ mm$^{-1}$, average cosine of scattering angle $g=0.935$, and thickness $t=10$ mm) comprised of monodispersed spherical scatterers ($D=1.40$ $\mu$m, $n_s=1.59$, and $n_m=1.34$). The incident light was horizontally ($0^\circ$) polarized (Stokes vector $[1\ 1\ 0\ 0]^T$) and the Stokes parameters *[I Q U V]* of light exiting the sample through the backscattering plane ($X$-$Y$ plane, $Z=0$) were recorded in the simulation (the detection positions in the backscattering plane are shown in the inset). The rotation of the linear polarization vector ($\alpha$) was calculated from the Stokes parameters as[15]

$$\alpha = 0.5 \tan^{-1}(U/Q). \tag{6}$$

This large change in the orientation angle of the polarization vector caused by the scattering process can manifest as optical rotation (as evident from the figure) and would thus swamp the relatively small rotation $\psi$ of the polarization vector arising from the presence of chiral substances in a turbid medium.

In order to understand the origin of such scattering-induced rotation, we show the Monte Carlo-generated complete 16 element ($4\times4$) Mueller matrices from the same nonbirefringent, achiral, turbid medium. The photon detection geometry is the same as that shown in the inset of Fig. 1. The recorded Mueller matrices from two different positions in the backscattering plane ($X$-$Y$ plane, $Z=0$, position 1: coordinate (1,1) and position 2: coordinate (2,0)] are

$$\text{matrix 1:}\begin{pmatrix} 1.0000 & 0.0003 & 0.1015 & -0.0011 \\ -0.0002 & -0.0681 & 0.0009 & 0.0735 \\ -0.1011 & 0.0010 & -0.2258 & 0.0009 \\ 0.0007 & 0.0744 & -0.0018 & 0.4464 \end{pmatrix}, \tag{7}$$

$$\text{matrix 2:}\begin{pmatrix} 1.0000 & -0.0690 & 0.0002 & -0.0034 \\ -0.0666 & 0.2192 & 0.0012 & -0.0035 \\ -0.0004 & 0.0018 & 0.1407 & -0.0535 \\ 0.0012 & -0.0012 & 0.0568 & 0.4674 \end{pmatrix}. \tag{8}$$

It is evident that when Matrix 1 is applied on input Stokes vector $[1\ 1\ 0\ 0]^T$ (incident horizontally polarized light), the nonzero matrix elements **M** (1,3) and **M** (3,1) lead to a nonzero value for the third Stokes parameter $U$ and this manifests as apparent optical rotation [$\alpha=27.85^\circ$ calculated using Eq. (6)]. Similarly, the nonzero elements **M** (1,2) and **M** (2,1) of matrix 2 will lead to apparent optical rotation when applied on input Stokes vector $[1\ 0\ 1\ 0]^T$ ($\alpha=12.50^\circ$ for incident $+45^\circ$ polarized light).

Note that the Mueller matrix elements **M** (1,2) and **M** (1,3) represent linear diattenuation for horizontal (vertical) and $+45^\circ$ ($-45^\circ$) linear polarizations, respectively. Further, pure optical rotation that arises from circular birefringence property (chirality) of the medium should manifest a difference between the Mueller matrix elements **M** (3,2) and **M** (2,3) [see Eq. (4)]. Since the scattering induced rotation does not originate from circular birefringence effects [as evident from the elements **M** (3,2) and **M** (2,3) of matrix 1 and matrix 2 from achiral turbid medium] but arises due to linear diattenuation, this can be decoupled from the pure optical rotation component using the polar decomposition of Mueller matrix. This is illustrated in Table I, where the results of decomposition of the Mueller matrix 2 are presented. The values for the different polarization parameters (diattenuation $d$, depolarization coefficient $\Delta$, optical rotation $\psi$, and linear retardance $\delta$) derived from the decomposed matrices via Eqs. (2)–(5) are also listed in the table. As expected, the decomposition process yields appreciable values for diattenuation ($d=0.069$); however, there is no significant component of optical rotation ($\psi=0.009^\circ$) from this achiral turbid medium.

Downloaded 08 Oct 2009 to 146.139.50.17. Redistribution subject to AIP license or copyright; see http://jap.aip.org/jap/copyright.jsp

TABLE II. Top: The Monte Carlo simulation generated Mueller matrix and the decomposed basis matrices for a nonbirefringent ($\Delta n=0$), achiral ($\chi=0°$ cm$^{-1}$), turbid medium ($\mu_s=6$ mm$^{-1}$ and $g=0.935$). The Mueller matrix was recorded in the backward detection geometry at a distance 5 mm ($r>l_{tr}$) away from the point of illumination [position coordinate (5,0), $Z=0$]. Bottom: The values for the different polarization parameters extracted from the decomposed matrices via Eqs. (2)–(5).

$$\mathbf{M}=\begin{pmatrix} 1.0 & -0.0178 & 0.0057 & 0.0043 \\ -0.0171 & 0.1376 & 0.0014 & 0.0035 \\ 0.0009 & 0.0016 & 0.1368 & -0.0091 \\ -0.0013 & -0.0009 & 0.0166 & 0.4354 \end{pmatrix}$$

$$\mathbf{M}_{\Delta}=\begin{pmatrix} 1.0 & 0 & 0 & 0 \\ -0.0147 & 0.1387 & 0 & 0 \\ 0.0002 & 0 & 0.1357 & 0 \\ -0.0033 & 0 & 0 & 0.4358 \end{pmatrix}$$

$$\mathbf{M}_{\mathbf{R}}=\begin{pmatrix} 1.0 & 0 & 0 & 0 \\ 0 & 1.0 & -0.0006 & 0.0080 \\ 0 & 0.0009 & 0.9990 & -0.0449 \\ 0 & -0.0080 & 0.0449 & 0.9990 \end{pmatrix}$$

$$\mathbf{M}_{\mathbf{D}}=\begin{pmatrix} 1.0 & -0.0178 & 0.0057 & 0.0043 \\ -0.0178 & 1.0 & -0.0001 & -0 \\ 0.0057 & -0.0001 & 0.9998 & 0 \\ 0.0043 & -0 & 0 & 0.9998 \end{pmatrix}$$

| Parameters | Estimated values |
|---|---|
| $d$ | 0.019 |
| $\Delta$ | 0.763 |
| $\psi$ | 0.02° |
| $\delta$ | 0.045 rad |

Note that in addition to diattenuation, the decomposition process also yields a significant value for linear retardance $\delta$ [as seen from the nonzero elements $\mathbf{M_R}$ (3,4) and $\mathbf{M_R}$ (4,3)] even though this is an isotropic sample with $\Delta n=0$. This scattering-induced linear retardance would interfere with the actual retardance values of a birefringent turbid medium in a complex interrelated way, thus hindering the determination of the latter in the backward detection geometry.

The scattering-induced diattenuation and linear retardance arise from the differences in amplitude and phase between the scattered light polarized parallel and perpendicular to the scattering plane, and are due mainly to the singly (or weakly) backscattered photons.[16] The magnitude of these single/few scattering-induced effects depends on the size parameter of the scatterer and increases at large scattering angles (scattering angle angle$>30°$, here scattering angle is defined with respect to the forward direction). A major contribution of the photons detected near the exact backscattering direction [radial distance $r<l_{tr}$, $l_{tr}$ is the transport scattering length$=1/\mu_s(1-g)$] are from backscattered photons, which have not undergone significant number of scattering events. The contribution of these singly/weakly backscattered photons results in significant values for linear retardance and diattenuation at detection positions sufficiently close to the exact backscattering direction [for the results shown in Table I, $r$(=2 mm)$<l_{tr}$(=2.56 mm)]. The contribution of these backscattered photons can also be identified by examining the elements of the decomposed depolarization matrix $\mathbf{M_\Delta}$ of Table I. If multiply scattered photons were the dominant contributor, the linear depolarization coefficients should have been independent of the incident linear polarization vector $[\mathbf{M_\Delta}(2,2)\sim\mathbf{M_\Delta}(3,3)]$ due to randomization process.[26] However, the values for the linear depolarization coefficients of incident horizontal (or vertical) and +45° (or −45°) linearly polarized light are observed to be significantly different $[\mathbf{M_\Delta}(2,2)>\mathbf{M_\Delta}(3,3)]$ at this detection position. While exact backscattering does affect horizontally (or vertically) polarized light significantly, it transforms +45° linearly polarized light to −45° polarized light or vice versa (a phenomenon similar to the helicity flipping of circularly

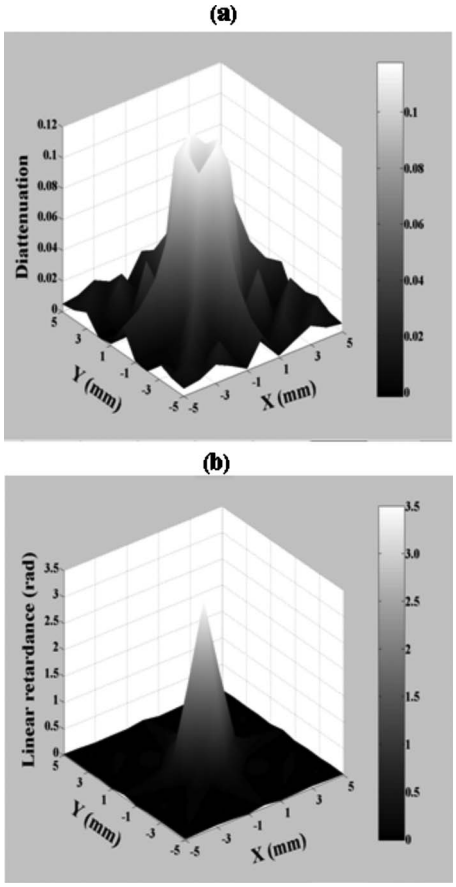


FIG. 2. (a) Diattenuation $d$ and (b) linear retardance $\delta$ maps in the backscattering plane ($X$-$Y$ plane, $Z=0$) derived using decomposition of Monte Carlo-generated Mueller matrices of a nonbirefringent ($\Delta n=0$), achiral ($\chi=0°$ cm$^{-1}$), turbid medium ($\mu_s=6$ mm$^{-1}$ and $g=0.935$).

Downloaded 08 Oct 2009 to 146.139.50.17. Redistribution subject to AIP license or copyright; see http://jap.aip.org/jap/copyright.jsp

TABLE III. Top: The Monte Carlo-generated Mueller matrix and the decomposed basis matrices for a birefringent, chiral, turbid medium ($\Delta n = 1.36 \times 10^{-5}$, which corresponds to a value of $\delta = 1.35$ rad for a pathlength of 10 mm, optical activity $\chi = 1.96°$ cm$^{-1}$, $\mu_s = 6$ mm$^{-1}$, and $g = 0.935$). The axis of linear birefringence was kept along the vertical ($Y$) direction (orientation angle $\theta = 90°$) in the simulation and the results are shown for scattered light collected at a spatial position 5 mm ($r > l_{tr}$) away from the point of illumination along the horizontal ($X$)-axis (see inset of Fig. 1 for geometry). Bottom: The values for the different polarization parameters extracted from the decomposed matrices via Eqs. (2)–(5).

**M**

| | | | |
|---|---|---|---|
| 1.0 | −0.0167 | −0.0019 | −0.0095 |
| −0.0190 | 0.1273 | 0.0075 | −0.0058 |
| 0.0009 | −0.0054 | 0.0302 | −0.1853 |
| 0.0024 | −0.0051 | 0.1901 | 0.2648 |

**$M_\Delta$**

| | | | |
|---|---|---|---|
| 11.0000 | 0 | 0 | 0 |
| −0.0169 | 0.1215 | 0 | 0 |
| −0.0009 | 0 | 0.1275 | 0 |
| 0.0052 | 0 | 0 | 0.3562 |

**$M_R$**

| | | | |
|---|---|---|---|
| 1.0 | 0 | 0 | 0 |
| 0 | 0.9978 | 0.0590 | −0.0289 |
| 0 | −0.0591 | 0.6159 | −0.7856 |
| 0 | −0.0286 | 0.7856 | 0.6181 |

**$M_D$**

| | | | |
|---|---|---|---|
| 1.0 | −0.0167 | −0.0019 | −0.0095 |
| −0.0167 | 1.0 | 0 | 0.0001 |
| −0.0019 | 0 | 0.9998 | 0 |
| −0.0095 | 0.0001 | 0 | 0.9999 |

| Parameters | Estimated values |
|---|---|
| $d$ | 0.019 |
| $\Delta$ | 0.798 |
| $\psi$ | 2.09° |
| $\delta$, $\theta$ | 0.905 rad, 88.9° |

polarized light).[27] This contributes to the observed lower value for the depolarization coefficient $\mathbf{M_\Delta}$ (3,3) at detection position $r < l_{tr}$.

When detection is performed at a distance larger than a transport length away from the point of illumination ($r > l_{tr}$), the contribution of the singly/weakly backscattered photons is reduced. In these cases, the detected signal from a forward scattering medium ($g \geq 0.9$) is primarily composed of the multiply scattered photons that have undergone a series of forward scatterings to emerge from the medium in the backward direction. Due to the reduced contribution of the singly/weakly scattered photons, the scattering-induced linear retardance and diattenuation effects will be reduced. This can be seen from Table II where the results of decomposition of Monte Carlo-generated Mueller matrix are shown for backward detection geometry at a distance of 5 mm ($r > l_{tr}$) away from the point of illumination. As expected, due to the dominant contribution of multiply scattered photons, linear depolarization coefficient of the decomposed depolarization matrix is found to be independent of the orientation angle (horizontal, vertical, and 45°) of the incident linear polarization vector [$\mathbf{M_\Delta}(2,2) \sim \mathbf{M_\Delta}(3,3)$].

The diattenuation ($d$) and linear retardance ($\delta$) maps in the backscattering plane ($X$-$Y$ plane, $Z=0$) from the nonbirefringent ($\Delta n = 0$), achiral ($\chi = 0°$ cm$^{-1}$), turbid medium ($\mu_s = 6$ mm$^{-1}$, $g = 0.935$, and thickness $t = 10$ mm) are shown in Figs. 2(a) and 2(b), respectively. These results and further decomposition analyses of Monte Carlo-generated Mueller matrices for turbid media having different scattering coefficients $\mu_s$ confirmed that in the backward detection geometry, the effects of scattering-induced linear retardance and diattenuation are weak ($\delta \leq 0.1$ and $d \leq 0.03$) for detection positions located at distances larger than a transport length away from the point of illumination ($r > l_{tr}$). The Mueller matrices recorded at such geometries may thus be used for simultaneous determination of the intrinsic values for $\delta$ and $\psi$ of a birefringent, chiral, turbid medium, with minimal interference from scattering-induced effects.

To explore this finding further, Mueller matrices were generated at different spatial positions in the backscattering plane. Table III presents the Monte Carlo-generated Mueller matrix and the decomposed matrices for a birefringent, chiral, turbid medium ($\Delta n = 1.36 \times 10^{-5}$, which corresponds to a value of $\delta = 1.35$ rad for a pathlength of 10 mm, optical activity $\chi = 1.96°$ cm$^{-1}$, $\mu_s = 6$ mm$^{-1}$, and $g = 0.935$). The axis of linear birefringence was kept along the vertical ($Y$) direction (orientation angle $\theta = 90°$) in the simulation and the results are shown for scattered light collected at a spatial position 5 mm ($r > l_{tr}$) away from the point of illumination along the horizontal ($X$)-axis (see inset of Fig. 1 for geometry). The elements of the depolarization matrix $\mathbf{M_\Delta}$ and the resulting value for the depolarization coefficient $\Delta$ are close to the corresponding values for the nonbirefringent, achiral, turbid medium having the same scattering coefficient $\mu_s$, results of which were presented in Table II (difference in the value for $\Delta \sim 10\%$). The results for diattenuation $d$ are also in close agreement. The decomposition process thus successfully decouples the scattering induced depolarization and diattenuation effects and retrieves the intrinsic values for the parameters $\delta$ (and $\theta$) and $\psi$.

Figure 3(a) shows the variations in $\delta$ and $\psi$ (derived from the decomposition process) as a function of distance from the point of illumination (in the backscattering plane) for the same turbid medium ($\mu_s = 6$ mm$^{-1}$ and $g = 0.935$). The results are shown for two different values of linear birefringence ($\Delta n = 1.36 \times 10^{-5}$ and $0.68 \times 10^{-5}$, corresponding to values of $\delta = 1.35$ and 0.675 rad, respectively for a pathlength of 10 mm) and optical activity ($\chi = 1.96$ and 3.92° cm$^{-1}$), for scattered light collected at different spatial positions along the horizontal ($X$)-axis. The inset shows the

Downloaded 08 Oct 2009 to 146.139.50.17. Redistribution subject to AIP license or copyright; see http://jap.aip.org/jap/copyright.jsp

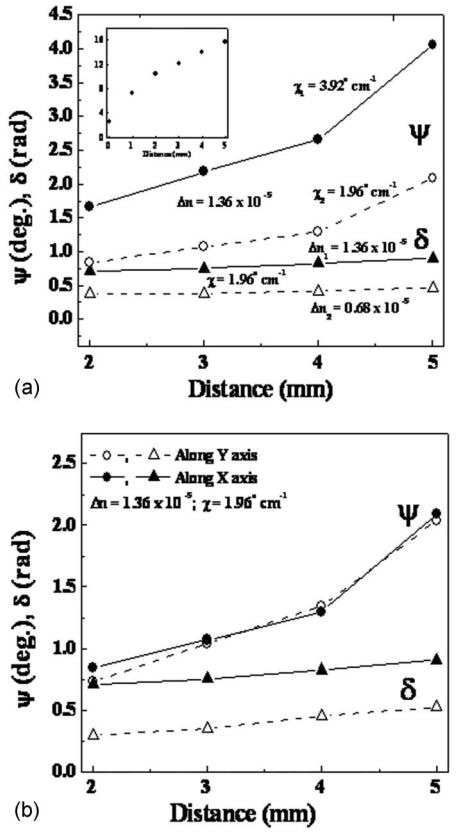


FIG. 3. (a) The variation of the values for Mueller matrix-derived $\delta$ and $\psi$ parameters as a function of distance from the point of illumination (in the backscattering plane, the detection geometry is the same as shown in the inset of Fig. 1) of a turbid medium ($\mu_s$=6 mm$^{-1}$, g=0.935). The results are shown for two different values of linear birefringence ($\Delta n = 1.36\times10^{-5}$ and $0.68\times10^{-5}$, with optical activity fixed at $\chi$=1.96° cm$^{-1}$) and optical activity ($\chi$=1.96 and 3.92° cm$^{-1}$, with linear birefringence fixed at $\Delta n = 1.36\times10^{-5}$). The axis of linear birefringence was kept along the vertical ($y$) direction (orientation angle $\theta$=90°) and the results are for scattered light collected at different spatial positions along the horizontal ($x$)-axis. The inset shows the Monte Carlo-calculated average photon pathlength as a function of the off-axis distance (both in mm). (b) The variation of the values for the Mueller matrix-derived parameters $\delta$ and $\psi$ as a function of the distance from the point of illumination (in the backscattering plane) along both the horizontal ($X$-axis, perpendicular to the direction of the linear birefringence axis) and vertical ($Y$-axis, parallel to the direction of the linear birefringence axis) directions for a birefringent ($\Delta n = 1.36\times10^{-5}$) chiral ($\chi$ =1.96° cm$^{-1}$) turbid medium $\mu_s$=6 mm$^{-1}$ and $g$=0.935.

Monte Carlo-calculated average photon pathlength as a function of the off-axis distance.[28,29] The value for $\psi$ is seen to increase with increasing average photon pathlength. However, the absolute values for $\psi$ are lower as compared to that expected from the linear relationship ($\psi=\chi\times$average photon pathlength). The Mueller matrix decomposed $\psi$ values from the same birefringent, chiral, turbid medium in the forward detection geometry were reasonably close to those calculated using this relationship.[13] Two factors contribute to the observed lower value for $\psi$ in the backward detection geometry as compared to that for the forward detection geometry. First, there is always some contribution of the singly/weakly backscattered photons in this geometry (more contribution at distances $r<l_{tr}$). For the photons that undergo a series of forward scattering events and eventually emerge in the backward direction, the optical rotation values at individual scattering steps add up to yield a large value of $\psi$; however, for the backscattered photons (that suffer scattering in the backward direction only), the net rotation value cancels out due to a change in the handedness of rotation (in the limit exactly retraced paths, the accrued optical rotation would be zero: This happens in a clear chiral medium with a reflective front surface, where the reflected linearly polarized beam that had traversed the medium twice has a net rotation of zero). Contribution of these backscattered photons thus reduces the value for net optical rotation $\psi$ in the backward detection geometry. Second, since the contribution of large angle scattered photons is greater in backward versus forward geometry, the propagation path of the polarization-preserving photons are shortened to a greater extent than the average photon pathlength, which has contribution of both the polarization-preserving and the depolarized photons.[28,29]

It is also pertinent to note that although the value for $\delta$ increases slightly with increasing average photon pathlength, the increase is much slower as compared to $\psi$. A similar trend was also observed for the forward detection geometry.[13] This is because in a turbid medium, the scattered light does not travel in a straight line but rather along many possible curved zigzag paths, the curvature being controlled by the values for $\mu_s$ and $g$. While such paths influence $\psi$ by increasing its value through a relationship with the increasing photon pathlength, the effect of this on the net value for $\delta$ will be more complex because a component of the curved propagation paths will be along the direction of the linear birefringence axis (orientation angle $\theta$=90° in the simulations).

Examining this further, the variations of the decomposition-derived parameters $\delta$ and $\psi$ are shown in Fig. 3(b) for the birefringent ($\Delta n = 1.36\times10^{-5}$), chiral ($\chi$ =1.96° cm$^{-1}$), turbid medium ($\mu_s$=6 mm$^{-1}$ and $g$=0.935). Here, the variations are shown as a function of the distance from the point of illumination (in the backscattering plane) along both the horizontal ($X$-axis, perpendicular to the direction of the linear birefringence axis) and vertical ($Y$-axis, parallel to the direction of the linear birefringence axis) directions. While the value for $\psi$ is found to be similar for detection positions located at the same distance either along the $Y$- or the $X$-axis, the value for $\delta$ is observed to be lower for detection at spatial positions along the $Y$-axis as compared to that along the $X$-axis. For the former case, a larger component of the photon propagation path is along the direction of the axis of birefringence and this leads to a reduction in the value for net linear retardance $\delta$ (because propagation along the direction of the birefringence axis does not yield any retardance).[13] The results of simulations for varying orientation angle of the linear birefringence axis ($\theta$) confirmed that while the derived value for $\psi$ is not influenced by a change in the value for $\theta$ of a birefringent, chiral, turbid medium, the maximum value for $\delta$ is obtained when detection is performed at spatial positions away (distance $r>l_{tr}$) from the point of illumination and perpendicular to the direction of the birefringence axis of the medium. It is of note that the decomposition of Mueller matrix yields values for both the magnitude of linear retardance $\delta$ and its orientation angle $\theta$. For biological tissue where *a priori* information on

Downloaded 08 Oct 2009 to 146.139.50.17. Redistribution subject to AIP license or copyright; see http://jap.aip.org/jap/copyright.jsp

the birefringence orientation angle will not be available, the optimal detection position can be decided from the polar-decomposition-derived value for orientation angle of linear retardance $\theta$. In fact, determination of $\theta$ and its variation in tissue could form a useful biological metric, either by itself or in conjunction with $\delta$-values describing the structural anisotropy of tissue.

## IV. CONCLUSIONS

We have investigated the efficacy of Mueller matrix decomposition method for simultaneous determination of the intrinsic values for linear retardance ($\delta$) and optical rotation ($\psi$) of a birefringent, chiral, turbid medium in backward detection geometry. The decomposition of the Monte Carlo-generated Mueller matrices revealed that near the exact backscattering direction (radial distance from the point of illumination $r <$ transport length $l_{tr}$), the influence of the scattering-induced effects (linear retardance and diattenuation) on the intrinsic values for $\delta$ and $\psi$ is significant, due to contribution of the backscattered photons. In contrast, these effects were observed to be significantly reduced for detection positions located at distances larger than a transport length ($r > l_{tr}$) away from the point of illumination. Simultaneous determination of the intrinsic values for $\delta$ and $\psi$ of a birefringent, chiral, turbid medium in the backward detection geometry can thus be accomplished by decomposing the Mueller matrix recorded at a distance larger than a transport length away from the point of illumination. Linear birefringence and optical activity are two common phenomena exhibited in biological tissue, and their determination in the backscattering geometry that is convenient for *in situ* applications should prove valuable in diagnostic photomedicine.

## ACKNOWLEDGMENTS

The Natural Sciences and Engineering Research Council of Canada and the Ontario Graduate Scholarship program are gratefully acknowledged for their financial support. The authors would also like to thank Dr. Daniel Cote for his help in developing the polarization-sensitive Monte Carlo code.

[1] L. V. Wang, G. L. Coté, and S. L. Jacques, J. Biomed. Opt. **7**, 278 (2002).
[2] P. J. Wu and J. T. Walsh, Jr., J. Biomed. Opt. **11**, 014031 (2006).
[3] D. J. Maitland and J. T. Walsh, Jr., Lasers Surg. Med. **20**, 310 (1997).
[4] J. F. de Boer, T. E. Milner, M. J. C. van Gemert, and J. S. Nelson, Opt. Lett. **22**, 934 (1997).
[5] R. J. McNichols and G. L. Cote, J. Biomed. Opt. **5**, 5 (2000).
[6] Q. Wan, G. L. Coté, and J. B. Dixon, J. Biomed. Opt. **10**, 024029 (2005).
[7] D. Cote and I. A. Vitkin, J. Biomed. Opt. **9**, 213 (2004).
[8] R. R. Ansari, S. Bockle, and L. Rovati, J. Biomed. Opt. **9**, 103 (2004).
[9] K. C. Hadley and I. A. Vitkin, J. Biomed. Opt. **7**, 291 (2002).
[10] I. A. Vitkin, R. D. Laszlo, and C. L. Whyman, Opt. Express **10**, 222 (2002).
[11] R. A. Chipman, *Handbook of Optics*, 2nd ed., edited by M. Bass (McGraw-Hill, New York, 1994), Chap. 22, Vol. 2, pp. 22.1–22.37.
[12] C. Brosseau, *Fundamentals of Polarized Light: A Statistical Optics Approach* (Wiley, New York, 1998).
[13] N. Ghosh, M. F. G. Wood, and I. A. Vitkin, J. Biomed. Opt. **13**, 044036 (2008).
[14] X. Guo, M. F. G. Wood, and I. A. Vitkin, J. Biomed. Opt. **11**, 041105 (2006).
[15] D. Côté and I. A. Vitkin, Opt. Express **13**, 148 (2005).
[16] S. Manhas, M. K. Swami, P. Buddhiwant, N. Ghosh, P. K. Gupta, and K. Singh, Opt. Express **14**, 190 (2006).
[17] D. Côté and I. A. Vitkin, available online at http://www.novajo.ca/ont-canc-instbiophotonics/.
[18] M. F. G. Wood, X. Guo, and I. A. Vitkin, J. Biomed. Opt. **12**, 014029 (2007).
[19] L. Wang, S. L. Jacques, and L. Zheng, Comput. Methods Programs Biomed. **47**, 131 (1995).
[20] C. F. Bohren and D. R. Huffman, *Absorption and Scattering of Light by Small Particles* (Wiley, New York, 1983), Chap. 2.
[21] R. Clark Jones, J. Opt. Soc. Am. **38**, 671 (1948).
[22] D. S. Kliger, J. W. Lewis, and C. E. Randall, *Polarized light in Optics and Spectroscopy* (Academic, New York/Harcourt Brace Jovanovich, New York, 1990), Chap. 5.
[23] S. Yau Lu and R. A. Chipman, J. Opt. Soc. Am. A Opt. Image Sci. Vis **13**, 1106 (1996).
[24] J. Morio and F. Goudail, Opt. Lett. **29**, 2234 (2004).
[25] R. Ossikovski, A. De Martino, and S. Guyot, Opt. Lett. **32**, 689 (2007).
[26] M. K. Swami, S. Manhas, P. Buddhiwant, N. Ghosh, A. Uppal, and P. K. Gupta, Opt. Express **14**, 9324 (2006).
[27] A. D. Kim and M. Moscoso, Phys. Rev. E **64**, 026612 (2001).
[28] X. Guo, M. F. G. Wood, and I. A. Vitkin, Opt. Express **15**, 1348 (2007).
[29] X. Guo, M. F. G. Wood, and I. A. Vitkin, Opt. Commun. **281**, 380 (2008).

**Downloaded 08 Oct 2009 to 146.139.50.17. Redistribution subject to AIP license or copyright; see http://jap.aip.org/jap/copyright.jsp**